Measurements and modeling of air-broadening coefficients for the 6 band of CH 3 I

E Raddaoui, P Soulard, M Guinet, H Aroui, D Jacquemart

Measurements and modeling of air-broadening coefficients for the ν_6 band of CH_3I

E. Raddaoui [a,b], P. Soulard [a], M. Guinet [a], H. Aroui [b], D. Jacquemart [a]*

[a] Sorbonne Université, CNRS, MONARIS, UMR 8233, 4 place Jussieu, 75005 Paris, France

[b] Université de Tunis, Ecole Nationale Supérieure d'Ingénieurs de Tunis, Laboratoire de Spectroscopie et Dynamique Moléculaire, 5 Avenue Taha Hussein, Tunis, Tunisia

Number of Pages: 12
Number of Figures: 8
Number of Tables: 3
Supplementary materials (electronic files): 2

[*] Corresponding author: Emna Raddaoui (emna.raddaoui@upmc.fr)

Keywords: Methyl iodide; ν_6 band; Air-broadening coefficients; *J*-and *K*-rotational dependences; Updated line list.

Abstract

The ν_6 band of methyl iodide around 9.5 μm is studied in terms of air-broadening coefficients. A multi-spectrum fitting procedure is applied to Fourier transform spectra using various mixtures of CH_3I and air in order to retrieve air-broadening coefficients. The numerous measurements performed in this work allow to model the *J*-and *K*-rotational dependences of the measured air-broadening coefficients. This model reproduces the measured air-broadening coefficients within standard deviation (1SD) equal to 7 %. Comparisons with measurements from literature are performed.

1. Introduction

Methyl iodide is a gas of atmospheric interest that contributes to the destruction of the ozone layer [1,2]. It is the most abundant iodine-containing compound emitted primarily by the oceans [3]. This molecule is also known as a tracer for radioactive pollution of nuclear power plants.

Several works based on the analysis of Fourier transform (FT) CH_3I spectra and focused on CH_3I line parameters measurements and models for transitions of the ν_6 band have been recently published [4-9] including the study performed by our group on the analysis of line intensities and self-broadening coefficients [7]. One can also notice the recent work on measurements of line intensities of transitions belonging to the ν_5 and $\nu_3 + \nu_6$ bands [10].

The present work is focused on measurements of air-broadening coefficients from FT spectra recorded with various mixtures of CH_3I and dry-air from commercial samples. The present study is a continuation of a previous work [7].

Measurements from literature of O_2-and N_2-broadening coefficients have been used in the present work to derive air-broadening coefficients in order to be compared with the present measurements of air-broadening coefficients. Two sets of measured O_2-and N_2-broadening coefficients have been used. Hoffman and Davies [11] studied by tunable diode laser absorption spectroscopy 5 ${}^{P}Q$ sub-branches (with K = 2, 3, 4, 5, 6 and J values from 8 to 56) of the ν_5 band. The second set of measured O_2-and N_2-broadening coefficients comes from Attafi et al. [8-9] where measurements of these two coefficients have been performed for around 250 transitions using FT spectra.

The experimental conditions of the recorded spectra are presented in Section 2. Section 3 is dedicated to the measurements and their analysis. Comparisons with literature and discussion are presented in Section 4.

2. Experimental spectra

Fourier transform spectra have been recorded at room temperature with various mixtures of CH_3I and dry-air using the Bruker IFS 120 HR interferometer of MONARIS. The experimental conditions are summarized in Table 1. Note that a pure CH_3I spectrum from Ref. [7] has been used in order to be fitted together with the four spectra of CH_3I broadened by dry-air (see Section 3). The commercial liquid sample of methyl iodide was

furnished by Sigma-Aldrich with a stated purity greater or equal to 99%. Since no accurate purity is given by Sigma-Aldrich, no correction has been performed in the given amount of CH_3I presented in Table 1. For dry-air, a commercial gas sample from Alphagaz (80% of N_2 and 20% of O_2 with purity greater or equal to 99.999%) was used.

(Table 1)

The interferometer was equipped with a KBr beam splitter, a MCT photovoltaic detector, and a Globar source. A stainless cell of (67.0 ± 0.1) cm path length was used to record all spectra without any optical filter. The cell was equipped with KBr windows. The experimental conditions (pressures, temperatures, number of scans, spectral resolutions) are summarized in Table 1. For all recorded spectra, the nominal value of the radius of the beam inside the interferometer is equal to 0.575 mm and the focal distance of collimation is equal to 418 mm.

An overview of the CH_3I studied absorption region between 935 and 960 cm^{-1} is presented in Fig. 1. This figure illustrates the global structure of different ${}^{R}Q$, and ${}^{R}R$ sub-branches. The transitions are noted ${}^{\Delta K}\Delta J_K$ (J) where J and K are the rotational quantum numbers of the lower state of the transition (J and K will refer in the whole text to rotational quantum numbers of the lower state), and ΔK and ΔJ represent the variation of these quantum numbers between the upper and lower levels. In this figure, the sub-branch noted ${}^{R}Q_7$, for example, refers to various ${}^{R}Q_7$ (J) transitions with K=7, ΔK = +1 and ΔJ = 0. A very weak multiplicative channel, due to the cell windows, is observed in experimental spectra. The maximum peak-to-peak amplitude is about 2% with a period of 0.6 cm^{-1}. This channel has been taken into account by a fitted background modeled with a polynomial function of order 2.

(Figure 1)

For each spectrum, the cell was first filled with CH_3I gas waiting for the pressure to be stable after CH_3I sticking on the wall of the cell. Then, dry-air has been introduced and the total pressure has been measured after stabilization of the total pressure. The partial pressure of CH_3I and total pressure (CH_3I and dry-air) have been measured using Baratron gauges, one thermostated of 10 mbar with a stated accuracy equal to 0.12%, and another one of 100 mbar non thermostated with a stated accuracy equal to 0.25%. The partial pressure of dry-air is calculated as the difference of the total pressure and the partial pressure of CH_3I

before introduction of dry-air. We supposed that the sticking rate of CH_3I on the wall did not change before and after introducing dry-air. The temperature of the gas has been recorded using a platinum probe. Average temperatures are listed in Table 1 with accuracy of 0.5K.

The recorded interferograms have been Fourier transformed using the procedure included in the Bruker software OPUS Package [12], selecting a Mertz phase error correction. The spectra have not been numerically apodized. The various spectral resolutions for spectra 0-5 are given in Table 1. Note that the Bruker resolution corresponds to $0.9/\Delta max$, where Δmax is the maximum optical path difference. As explained in Ref. [7] the signal-to-noise ratio depends strongly on wavenumbers since the beginning of the studied region (around 850 cm^{-1}) is at the edge of our spectra. Therefore, around 850 cm^{-1} the signal-to-noise ratio is equal to 50 for spectrum 0, whereas it reaches 200 around 950 cm^{-1}. For air broadened spectra (#1-4, see Table 1), signal-to-noise ratio is between 60 and 100 around 850 cm^{-1} and reaches its maximum (between 220 and 300) around 950 cm^{-1}.

3. Measurements and analysis

A multi-spectrum fitting procedure [13] using a Voigt profile has been applied to experimental spectra described in Table 1. The self-broadening contribution has been taken into account by fixing the self-broadening coefficients. Since two studies [7,8] dealing with measurements of self-broadening coefficients have been performed recently for a large set of transitions of the ν_6 band, a comparison has been performed and is presented in Fig. 2. A systematic discrepancy of about 10-15% is observed between measurements and models of these two works. Note that the model of Ref. [8] is based on non-smooth coefficients explaining the breaks observed in the modeled self widths in Fig. 2. Comparisons with measurements of Hoffman and Davies [11] obtained for the ν_5 band are also presented in Fig. 2 showing a better agreement with Ref. [7] than with Ref. [8], except for $K = 2$ transitions where agreement is slightly better between Ref. [11] and Ref. [8] than between Ref. [11] and Ref. [7]. It has been finally decided to fix the self-broadening coefficients to the values calculated using smoothed coefficients of Table 4 from Ref. [7].

(Figure 2)

The line position of the transition has been fitted by neglecting shifting coefficients of CH_3I by CH_3I, and by air. The line intensity has been adjusted taking into account the slight temperature dependence between experimental spectra. Air-broadening coefficients were set free neglecting their temperature dependence since all temperatures are close to room temperature. The apparatus function takes into account the optical weighting of the boxcar function (aperture radius is equal to 0.575 mm and collimator focal length *f* is equal to 418mm) as performed in Ref. [7]. The apparatus function is calculated [13] for each fitted spectral range taking into account the fact that the optical weighting function is wavenumber dependent. No division by an empty cell spectrum was performed; the background of the experimental spectra has been modeled by a second order polynomial function on fitted spectral windows ranging from 0.04 to 0.25 cm^{-1} depending if transitions were isolated or not. Finally, air-broadening coefficients have been retrieved for 959 transitions belonging to the ν_6 band of CH_3I. The large set of measurements for transitions from $J = 1$ to 63 and $K = 0$ to 12 allowed to fit a model describing the observed *J*- and *K*-rotational dependences.

Spectrum of pure CH_3I (spectrum 0, see Table 1) has been added in the multi-spectrum fitting procedure in order to ease the fit of transitions that become blended in experimental spectra for which air pressure is increasing. Indeed, fitting a pure spectrum of CH_3I together with the broadened spectra, helps to fit line positions of overlapped or even non resolved transitions observed in broadened spectra. Moreover, it allows us to check the consistency between spectrum 0 (from Ref. [7]) and spectra 1-4 recorded recently with mixtures of CH_3I and dry-air.

The Doppler full-width at half-maximum (FWHM) is around 0.001 cm^{-1} at 900 cm^{-1} and 296K. For the mixtures of CH_3I and dry-air used to record spectra 1-4 (see Table 1), the air-width contributions are around 5 times larger than the self-width contributions. The spectral resolution has been chosen to have a FWHM of the apparatus function similar to the total line width estimated from Doppler and collisional widths. Spectral resolution varies from one experimental spectrum to the other but do not prevent simultaneous multi-spectrum fitting. A sample of a fitted spectral region for the five experimental spectra of Table 1 is given in Fig. 3. Let recall that with a multi-spectrum fitting procedure, the line parameters of a fitted transition are fixed to be the same for all fitted spectra, allowing then to observe eventual inconsistencies between fitted spectra through systematic residuals. As it can be observed in Fig. 3, no systematic signatures appear in the residual of one specific spectrum. The Voigt profile has been used and no systematic signatures in “W” shape centered on the transitions has been detected. The residuals do not exceed 4% peak-to-peak

as observed in Fig. 3. When using a single-spectrum fitting procedure these inconsistencies between partial pressures of fitted spectra are not taken into account since the broadening coefficients are set free independently in each spectrum. Consequently the single-spectrum fitting residuals obtained in Fig. 3 are slightly reduced comparing to the multi-spectrum fitting residuals. Note that slightly improved residuals from single-fitting procedure do not imply any improvement in the retrieval of the line parameters. The differences between residuals obtained with a single-spectrum and multi-spectrum procedures are due to slight inconsistencies between experimental conditions of fitted spectra, probably from the partial pressures of CH_3I and dry-air in the cell. Inconsistencies between partial pressures may be due to the fact that the quantity of CH_3I sticking on the wall depends on the introduced pressure of dry-air whereas the partial pressures have been calculated supposing that the quantity of CH_3I sticking on the wall did not change before and after introducing dry-air. Another explanation could be that some CH_3I may have escape from the cell during the introduction of dry-air. In the case of the fitted spectral region in Fig. 3, the air-broadening coefficients retrieved from single- or multi-spectrum fitting procedures are respectively equal to 0.1052 and 0.1062 cm^{-1} atm^{-1} for the first transition (0.9% difference), 0.1057 and 0.1019 cm^{-1} atm^{-1} for the second one (3.7% difference), 0.1071 and 0.1012 cm^{-1} atm^{-1} for the third one (5.8% difference), 0.1377 and 0.1330 cm^{-1} atm^{-1} for the fourth one (3.5% difference).

(Figure 3)

(Table 2)

The global uncertainty defined in Ref. [16] (accuracy term is often used, as in HITRAN [14] or GEISA [15] databases) into account both sources of systematic errors (accuracies) and sources of statistical errors.

The sources of systematic errors for broadening coefficients are the pressures read on Gauges (accuracy of 0.12-0.25%) and the absorption path length (accuracy of 0.2%). Some others systematic errors are more difficult to estimate such as an error on the line profile, on the exact partial pressure of the CH_3I and dry-air in the cell, or on the calculation of the apparatus function. Some errors depend either of the deepness of the observed lines (error linked to the profile or the apparatus function) or of the energy of the lower state of the transition (for an error on temperature T) and can reach a few percents. The systematic biases can be observed by models comparisons or by averaging numerous measurements.

When averaging numerous measurements, the global uncertainties should push towards those systematic biases (accuracy). For individual lines the systematic biases are negligible compared to the dispersion of the measurement (statistical uncertainty).

Statistical uncertainties are also difficult to estimate. The signal-to-noise ratio (from 50 to 300 depending on the spectrum and the spectral range, see Section 2) and the RMS (root mean squared) of the fitted parameters lead only to one part of the statistical errors. The choice of parameters that influences the fit of the calculated spectra (size of fitted spectral region, background model, single or multi-spectrum fitting procedure, unassigned transitions added in the fit, line parameters fixed or set free during the fit, inclusion of hyperfine structure…) plays also an important role in the statistical dispersion of the retrieved line parameters.

The global uncertainty of the measured air-broadening coefficients has not been calculated line by line but is estimated to be around 5-15%. This estimation encompasses the various experimental accuracies (0.2% on the pressure, 0.2% on the cell path, 0.2% on the temperature), the peak-to-peak level of noise between 0.3-2% of the signal, the mixing ratio of the two gases estimated to be around 1%, the RMS of the fitted parameter (0.5-10% for more than 99% of measurements, but can reach up to 30% for a few measurements: see supplementary material) but also what we call the noise of operator due to the choice of parameters that influence the fit (size of fitted spectral region, calculation of apparatus function, single or multi-spectrum fitting procedure, unassigned transitions added in the fit, line parameters fixed or free during the fit, …). The noise of operator is hard to estimate since it depends on each case. To our point of view it is hopeless to try to calculate global uncertainty for each fitted transitions. Only the RMS of the fitted parameter is given for each transition (see Table 2). The dispersion of our measurements compared with the model (see Figs. 4-8) gives a good estimation of these statistical errors. By using an appropriate model reproducing the global rotational dependence of the measurements, the statistical dispersion will be greatly reduced, and the global uncertainty of the modeled values will get closer to the systematic biases (accuracy).

Sample of measured air-broadening coefficients is listed in Table 2 and the whole set of measurements is given as supplementary material. Measurements of $K = 0$, 5 and 7 have been plotted versus J in Fig. 4 using different colors for different sub-branch types. No significant dependence on the type of sub-branches has been observed in this work. Note that for C_{3v} symmetric-top molecules as CH_3I, the symmetry of the rovibrational levels is $A_1/A_2/E$ depending on the vibrational state and the rotational quantum numbers J and K. For

K = 3, 6, 9 …, the two components A_1/A_2 are unresolved so that the two components are fitted as only one transition for which the symmetry is noted A.

(Figure 4)

Since no sub-branch dependence has been observed, the whole set of measurements has been used to model the J- and K-rotational dependences of the air-broadening coefficients based only on the values of the rotational quantum numbers J and K of the lower state of the transitions. For each set of measurements with same value of J, the following equation has been used:

$$\gamma_J(K) = a_J^0 + a_J^2 K^2 . \quad (1)$$

The a_J^0 parameters correspond to the broadening coefficients for K = 0 lines, whereas the a_J^2 parameters represent the K-rotational dependence of the width which is responsible of the decreasing of the width when K is increasing ($a_J^2 < 0$). The observed and modeled K-rotational dependences have been plotted in Fig. 5 for 4 sets of J values (J = 4, 8, 12 and 20) that show the decreasing of the a_J^2 parameter toward zero when J is increasing. The two coefficients a_J^0 and a_J^2 obtained from J = 3 to J = 60 are given in Table 3 and have been plotted in Fig. 6 with those deduced from the linear combination of parameters obtained in Refs. [8-9] for O_2- and N_2-broadening coefficients ($\gamma_{air} = 0.8\times\gamma_{N2} + 0.2\times\gamma_{O2}$). As it can be observed, the zero and second order coefficients obtained in this work present less dispersion than those of Refs. [8-9]. Note that for J values higher than 51, the transitions are quite weak in our experimental conditions so that the K rotational dependence could not be retrieved (a_J^2 parameter fixed to zero). Since they are smoothly J dependent, smoothed a_J^0 and a_J^2 parameters (red line in Fig. 6) have been generated by hand in order to reduce the experimental dispersion.

(Figure 5)

(Figure 6)

Global uncertainty on the modeled air-broadening coefficients is certainly reduced for most of the J and K values comparing to the one estimated for our measurements (5-15%). However, due to the strong J dependence for low J values, the global uncertainty of

the model may not be improved for the low *J* values close to *K*. The whole set of calculated air-broadening coefficients (using Eq. (1) and smoothed parameters of Table 3) are plotted versus *J* for *K* values ranging from 0 to 15 in Fig. 7 using various colors for each *K* values. These calculated air-broadening coefficients have been used to update the line list presented in Ref. [7] in HITRAN format [14], using error codes of 6 corresponding to an accuracy equal to 2-5% (global uncertainty according to terminology of Ref. [16]). The updated line list is available as supplementary data.

(Figure 7)

4. Comparisons with literature

Two sets of N_2 and O_2-broadening coefficients measurements have been compared to the present measurements of air-broadening coefficients. For that, air-broadening coefficients have been deduced from the linear combination of O_2- and N_2-broadening coefficients ($\gamma_{air} = 0.8\times\gamma_{N2} + 0.2\times\gamma_{O2}$). One set of N_2 and O_2-broadening coefficients measurements has been retrieved from the analysis of tunable diode laser spectra for transitions belonging to the ν_5 band [11]. The other set has been retrieved from the analysis of FT spectra for transitions of the ν_6 band [8-9]. Both analyses [8,9,11] have been performed using a Voigt profile. No accuracy is given for measurements of Ref. [11] but relative uncertainty is expected to be very good (around 1%) as it can be observed in Fig. 8 where the dispersion of the measurements is quite small as compared to the dispersion of present measurements and those of Refs. [8-9]. In Refs. [8-9] the accuracy has been calculated for each line and varies between 3.3 and 4.3% depending on the studied transitions. Such accuracies are, to our point of view, not consistent with observed dispersion of measurements from Refs. [8-9] that reach 15% (see Fig. 8). Note that the model proposed in Refs. [8-9] has not been plotted in Fig. 8 because of large breaks due to the fact that a_J^0 and a_J^2 parameters retrieved in Refs. [8-9] have not been smoothed.

(Figure 8)

Despite the large dispersion observed in Fig. 8 for the present measurements and those of Refs. [8-9] the two sets of measured air-broadening coefficients are consistent (see

Fig. 8). Comparisons with measurements of Ref. [11] lead to a similar conclusion even if for K= 3, 4, 5 and 6, the measurements of Ref. [11] are around 2% systematically lower than our model plotted in red in Fig. 8, but present similar rotational dependence. For K= 2, one can see that the rotational dependence modeled in the present work is less significant than the one observed in Ref. [11].

5. Conclusion

Air-broadening coefficients have been retrieved for 959 transitions belonging to the ν_6 band of CH_3I based on multi-spectrum fitting procedure of FT spectra using a Voigt profile. The large set of measurements allowed performing the study of J- and K-rotational dependences of the air widths. The derived model has been used to update the list for the ν_6 band of CH_3I published in our previous work [7]. The updated line list is available as supplementary material.

References

[1] Allan BJ, Mc Figgans G, Plane JMC, Coe H. Observation of iodine oxide in the remote marine boundary layer. J Geophys Res 2000;105:14363–70.

[2] Bell N, Hsu L, Jacob DJ, Schultz MG, Blake DK, Butler JH, King DB, Lobert JM, Maier-Reimer E. Methyl iodide: atmospheric budget and use as a tracer of marine convection in globel models. J Geophys Res 2002;107:1–12.

[3] Yokouchi Y, Nojiri Y, Toom-Sauntry D, Fraser P, Inuzuka Y, Tanimoto H, Nara H, Murakami R, Mukai H. Long-term variation of atmospheric methyl iodide and its link to global environmental change. Geophys Res Lett 2012;39:L23805.

[4] Haykal I, Doizi D, Boudon V, El Hilali A, Manceron L, Ducros G . Line positions in the v_6 =1 band of methyl iodide: Validation of the C_{3v}TDS package based on the tensorial formalism. J Mol Spectrosc 2016;173:13–19.

[5] Perrin A, Haykal I, Kwabia Tchana F, Manceron L, Doizi D, Ducros G. New analysis of the v_6 and $2v_3$ bands of methyl iodide (CH_3I). J Mol Spectrosc 2016;324:28–35.

[6] Kwabia Tchana F, Attafi Y, Manceron L, Doizi D, Vander Auwera J, Perrin A. Line intensities for the ν_6 and $2\nu_3$ bands of methyl iodide ($^{12}CH_3I$). J Quant Spectrosc Radiat Transfer 2019;222-223:130–37.

[7] Raddaoui E, Troitsyna L, Dudaryonok A, Soulard P, Guinet M, Aroui H, Buldyreva J, Lavrentieva N, Jacquemart D. Line parameters measurements and modeling for the v_6 band of CH_3I: A complete line list for atmospheric databases. J Quant Spectrosc Radiat Transf 2019;232**:** 165–179.

[8] Attafi Y, Ben Hassen A, Aroui H, Kwabia Tchana F, Manceron L, Doizi D, Vander Auwera J, Perrin A. Self and N_2 collisional broadening of rovibrational lines in the v_6 band of methyl iodide ($^{12}CH_3I$) at room temperature: The *J* and *K* dependence. J Quant Spectrosc Radiat Transfer 2019;231:1–8.

[9] Attafi Y, Galalou S, Kwabia Tchana F, Vander Auwera J, Ben Hassen A, Aroui H, Perrin A, Manceron L, Doizi D. Oxygen broadening and shift coefficients in the v_6 band of methyl iodide ($^{12}CH_3I$) at room temperature. J Quant Spectrosc Radiat Transfer 2019;239:106679.

[10] Boughdiri A, Manceron L, Maaroufi N, Rotger M, Aroui H. Measurments of line intensities for some lines of methyl iodide in the ν_5 and $\nu_3 + \nu_6$ bands. J Quant Spectrosc Radiat Transf 2018;221:147–54.

[11] Hoffman KJ, Davies PB. Pressure broadening coefficients of ν_5 fundamental band lines of CH_3I at 7 μm measured by diode laser absorption spectroscopy. J Mol Spectrosc 2008;252:101–07.

[12] Wartewig S. IR and Raman spectroscopy: fundamental processing. Weinheim: Wiley-VCH 2003.

[13] Lyulin O. Determination of Spectral Line Parameters from Several Absorption Spectra with the MultiSpectrum Fitting Computer Code. Atmospheric and Oceanic Optics 2015;28:487–95.

[14] Rothman LS, Gordon IE, Barbe A, Benner DC, Bernath PF, Birk M, et al. The HITRAN 2008 molecular spectroscopic database. J Quant Spectrosc Radiat Transf 2009;110**:**533–72.

[15] Jacquinet-Husson N, Crepeau L, Armante R, Boutammine C, et al. The 2009 edition of the GEISA spectroscopic database. J Quant Spectrosc Radiat Transf 2011;112:2395–445.

[16] Evaluation of measurement data – Guide to the expression of uncertainty in measurement. Document produced by Working Group 1 of the Joint Committee for Guides in Metrology. JCGM 100:2008.
Reference to a website : https://www.bipm.org/fr/publications/guides/

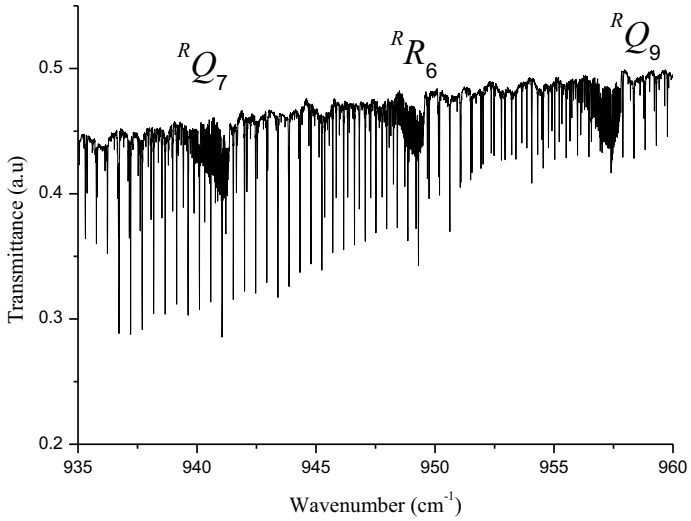

Figure 1: Overview of the ν_6 band in spectrum #3 (see Table 1) between 935 and 960 cm^{-1}.

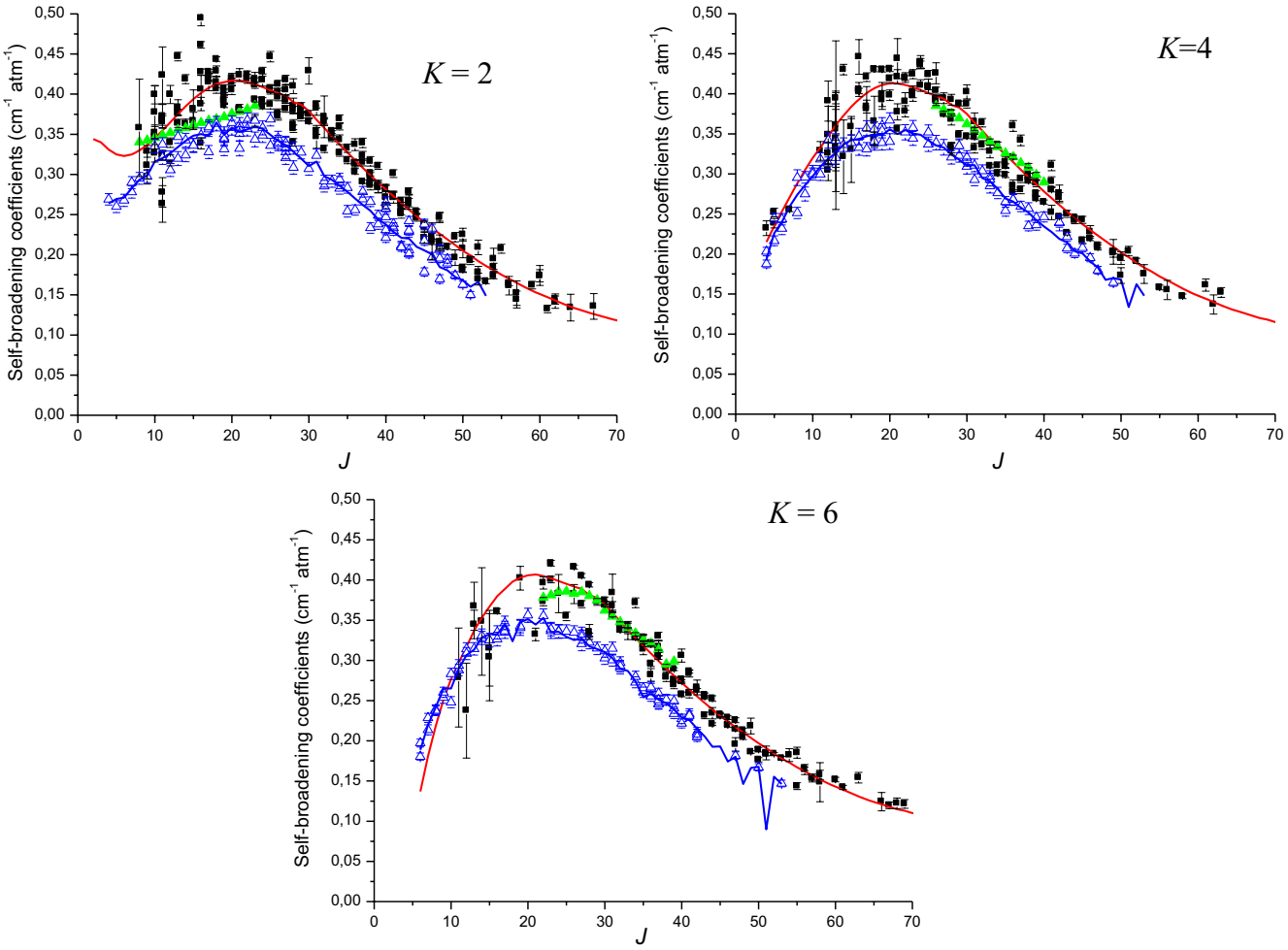

Figure. 2: Comparisons of self-broadening coefficients measured in Ref. [7] (black squares) and in Ref. [8] (blue triangles) for the ν_6 band of CH_3I with those measured for the ν_5 band from Ref. [11] (green triangles). Models from Ref. [7] and Ref. [8] are plotted as red and blue continuous line respectively.

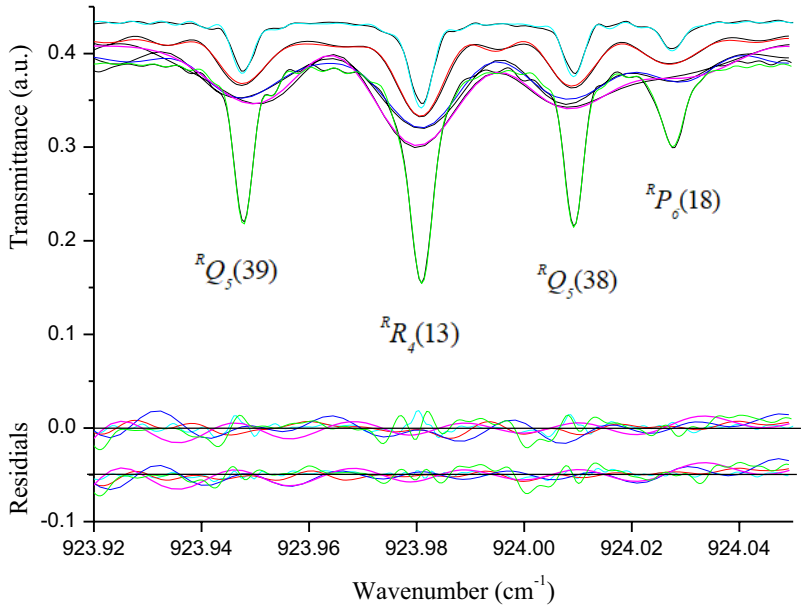

Figure 3: Multi-spectrum fitting of four transitions using 5 spectra: 1 of pure CH_3I and 4 with various mixtures of CH_3I and dry-air (see experimental conditions listed in Table 1). Centered on zero, the residuals (calc-obs)/calc have been plotted when performing a multi-spectrum fit. Centered on -0.05 are plotted residuals when performing a single-spectrum fit.

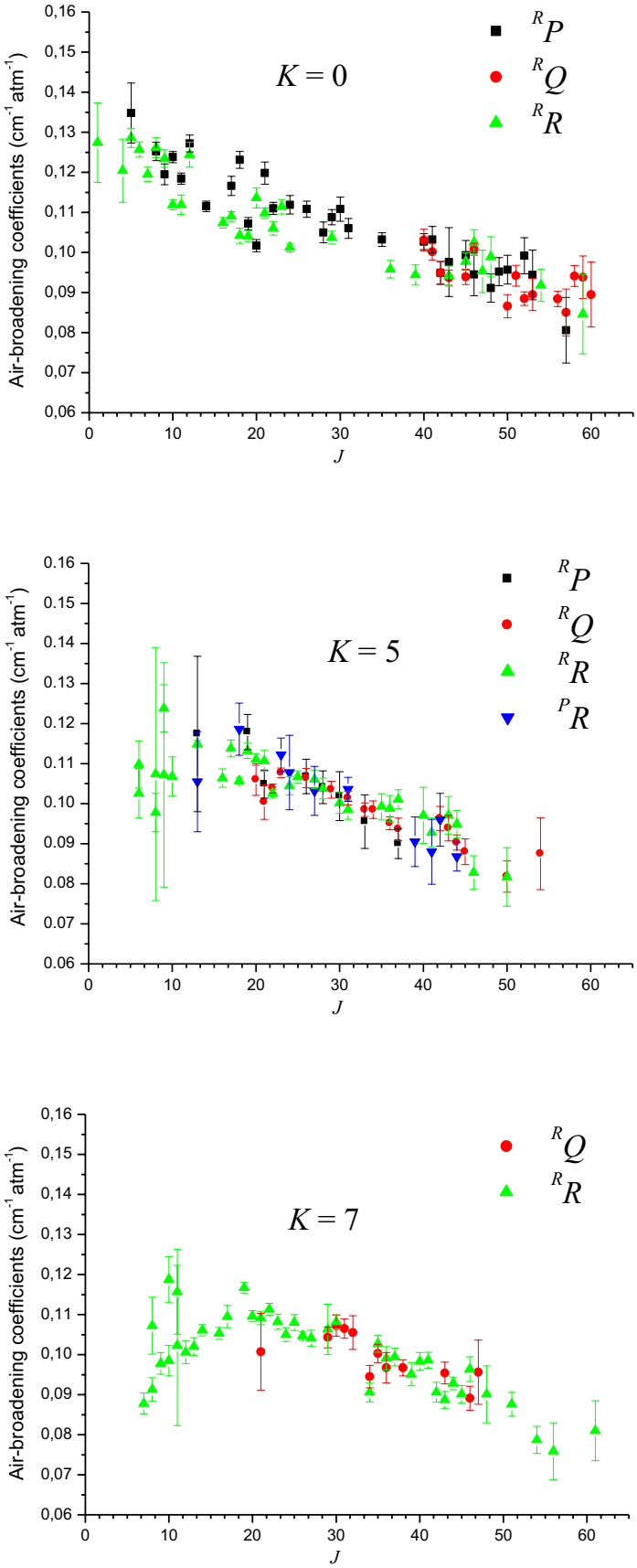

Figure 4: Measured air-broadening coefficients for K = 0, 5 and 7 plotted versus the rotational quantum number J. Different colors and symbols have been used to distinguish the various sub-branch types. The error bars correspond to the RMS of the fitted air-broadening coefficients.

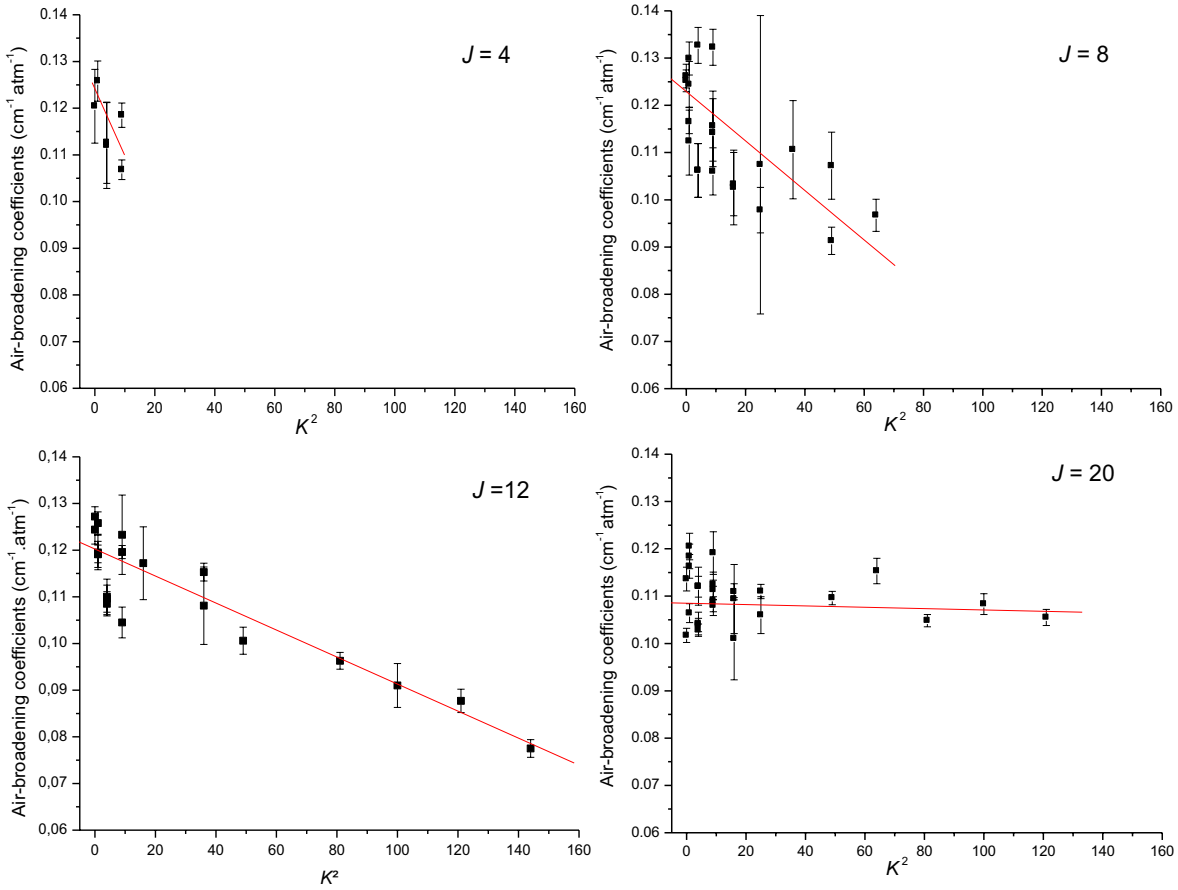

Figure 5: *K*-rotational dependences of the measured air-broadening coefficients for a set of same *J* value (*J* = 4, 8, 12, 20). The solid symbols represent the measured air-broadening coefficients whereas the continuous red line stands for the fit of the measurements using Eq. (1). The error bars correspond to the RMS of the fitted broadening parameters.

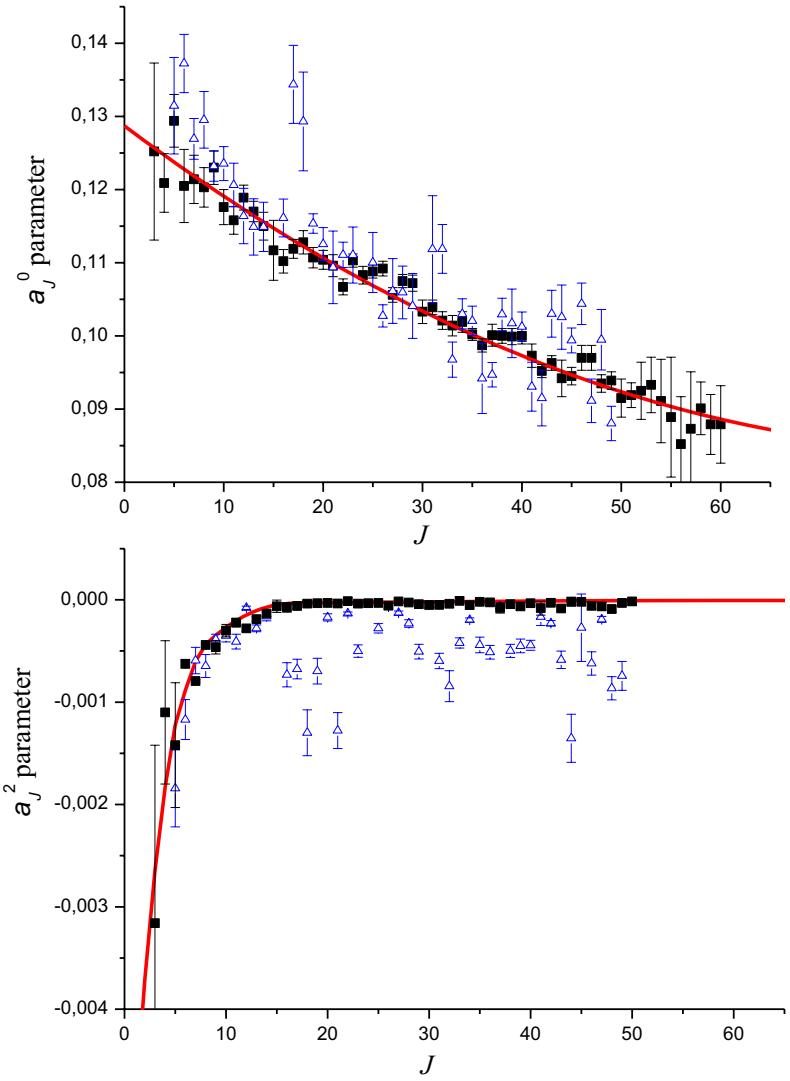

Figure 6: Parameters a_J^0 and a_J^2 (in cm^{-1} atm^{-1} at 296 K) deduced from the fit of the measured air-broadening coefficients using Eq. (1) (black squares). The continuous line represents the smoothed parameters obtained by hand and reported in Table 3. Blue triangles stand for air-parameters deduced from the linear combination of parameters obtained in Refs. [8,9] for O_2- and N_2-broadening coefficients ($\gamma_{air} = 0.8\times\gamma_{N2} + 0.2\times\gamma_{O2}$). The error bars correspond to 1SD deduced from the linear fit versus K^2 of Eq. (1) presented in Fig. 5.

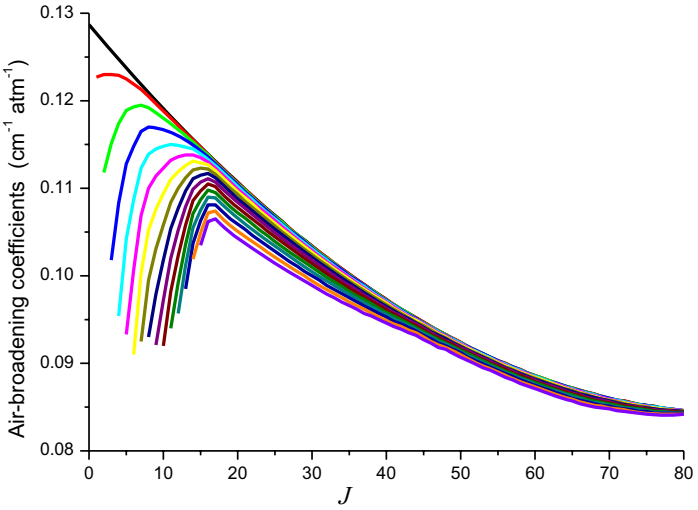

Figure 7: *J*-and *K*-rotational dependences of air-broadening coefficients calculated using Eq. (1) and smoothed parameters of Table 3.

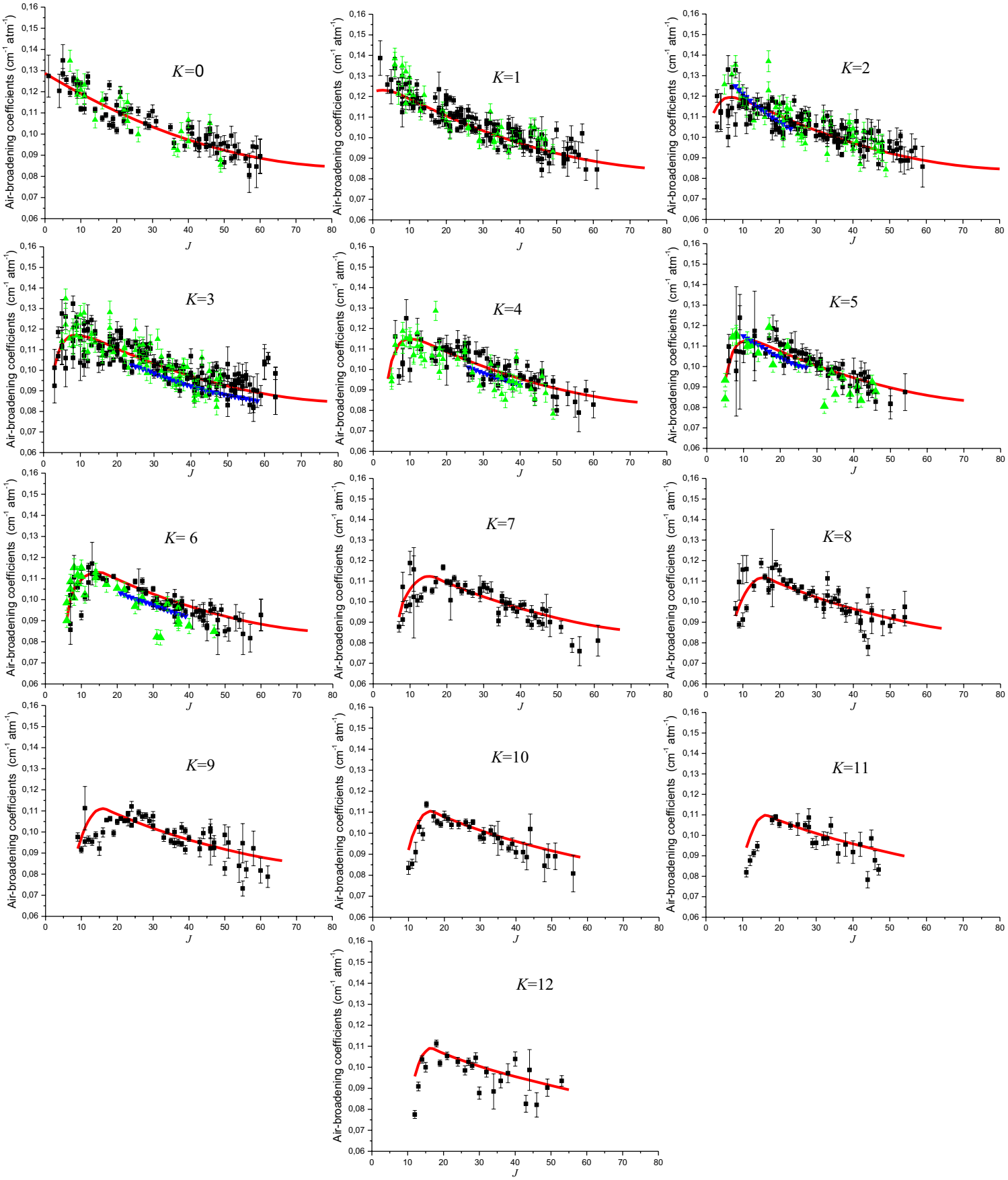

Figure 8: *J*-and *K*-rotational dependences of measured (solid squares) and calculated (red lines) air-broadening coefficients using Eq. (1) and smoothed parameters of Table 3. Green and blue triangles stand for a combination ($\gamma_{air} = 0.8\times\gamma_{N2} + 0.2\times\gamma_{O2}$) of measured N_2 and O_2-broadening coefficients for the ν_6 and ν_5 band of CH_3I in the work of [8,9] and [11] respectively. The error bars in the present work correspond to the RMS of the fitted parameters given in supplementary data whereas those from Ref. [8-9] correspond to accuracies given in Refs. [8-9].

Table 1 : Experimental conditions of the experimental spectra.

#	Pressure of CH_3I (mbar)	Pressure of dry-air (mbar)	Number of scans	Temperature (K)	Bruker resolution (cm^{-1})
0[a]	4.918	--	760	293.2	0.004
1	1.213	10.35	890	294.7	0.005
2	2.019	20.70	1610	294.6	0.010
3	2.933	31.90	840	293.9	0.015
4	5.061	40.34	990	293.6	0.020

[a] This spectrum has been previously recorded and analyzed in Ref. [7].

Table 2: Sample of fitted air-broadening coefficients in cm^{-1} atm^{-1} (between parentheses is 1SD in the last unit of the digit). The assignment column comports the branches type in column noted *Br* (first letter for ΔK. second letter for ΔJ), the rotational quantum numbers of the lower state of the transitions (*J* and *K*). and the symmetry of the lower level (Sym). The whole set of measured air-broadening coefficients is available as supplementary material.

Assignment				Air-broadening coefficients (cm^{-1} atm^{-1})
Br	*J*	*K*	Sym	
RR	1	0	A2	0.1274(99)
RR	4	0	A1	0.1204(79)
RR	5	0	A2	0.1286(24)
RP	5	0	A2	0.1348(75)
RR	6	0	A1	0.1257(19)
RR	7	0	A2	0.1195(18)
RP	8	0	A1	0.1252(23)
RR	8	0	A1	0.1262(25)
RR	9	0	A2	0.1234(22)
RP	9	0	A2	0.1195(26)
RR	10	0	A1	0.1119(12)
RP	10	0	A1	0.1238(14)
RP	11	0	A2	0.1184(14)
RR	11	0	A2	0.1119(24)
RP	12	0	A1	0.1272(21)
RR	12	0	A1	0.1244(31)
RP	14	0	A1	0.1115(13)
RR	16	0	A1	0.1074(13)
RR	17	0	A2	0.1090(12)
RP	17	0	A2	0.1166(24)
RR	18	0	A1	0.1042(19)
RP	18	0	A1	0.1231(21)
RR	19	0	A2	0.1040(13)
RP	19	0	A2	0.1072(15)
RP	20	0	A1	0.1017(15)
RR	20	0	A1	0.1136(25)
RR	21	0	A2	0.1098(13)
RP	21	0	A2	0.1198(28)
RP	22	0	A1	0.1110(15)
RR	22	0	A1	0.1060(17)
RR	23	0	A2	0.1114(18)
RR	24	0	A1	0.1012(11)
RP	24	0	A1	0.1119(23)
RP	26	0	A1	0.1108(20)
RP	28	0	A1	0.1050(26)
RR	29	0	A2	0.1037(16)
RP	29	0	A2	0.1088(19)
RP	30	0	A1	0.1108(30)
RP	31	0	A2	0.1060(25)
RP	35	0	A2	0.1032(17)
RR	36	0	A1	0.0958(22)
RR	39	0	A2	0.0944(25)

Table 3: Parameters a_J^0 and a_J^2 (in cm^{-1} atm^{-1}) retrieved for each set of air-broadening coefficients with same value of *J*. The second column of each parameter is used as substitutable smoothed or extrapolated values. Digits between parentheses represent 1SD (in the unit of the last digit) for the retrieved experimental a_J^0 and a_J^2 values. The column *N* corresponds to the number of measurements with same *J* value that have been fitted through Eq. (1) to obtain a_J^0 and a_J^2 parameters.

J	$a_{J\ \mathrm{exp}}^0$	$a_{J\ \mathrm{exp}}^2$	*N*	$a_{J\ \mathrm{smooth}}^0$	$a_{J\ \mathrm{smooth}}^2$
0				0.1287	-6.66E-3
1				0.1277	-5.04E-3
2				0.1267	-3.71E-3
3	0.1252(121)	-3.16E-3(174)	4	0.1257	-2.65E-3
4	0.1209(40)	-1.10E-3(70)	6	0.1247	-1.83E-3
5	0.1294(36)	-1.42E-3(61)	7	0.1238	-1.22E-3
6	0.1205(50)	-6.25E-4(40)	12	0.1228	-8.83E-4
7	0.1214(33)	-7.94E-4(13)	10	0.1219	-6.00E-4
8	0.1203(27)	-4.42E-4(11)	20	0.1209	-4.37E-4
9	0.1230(23)	-4.63E-4(66)	16	0.1200	-3.45E-4
10	0.1176(24)	-3.01E-4(61)	22	0.1191	-2.71E-4
11	0.1158(19)	-2.23E-4(41)	24	0.1182	-2.00E-4
12	0.1189(17)	-2.79E-4(31)	20	0.1173	-1.50E-4
13	0.1170(14)	-1.89E-4(25)	20	0.1164	-1.06E-4
14	0.1150(19)	-1.35E-4(27)	11	0.1156	-7.00E-5
15	0.1117(41)	-0.63E-4(60)	9	0.1147	-5.00E-5
16	0.1102(16)	-0.74E-4(46)	12	0.1139	-3.42E-5
17	0.1119(13)	-0.60E-4(30)	17	0.1131	-2.91E-5
18	0.1128(16)	-0.37E-4(30)	23	0.1123	-2.91E-5
19	0.1107(14)	-0.34E-4(26)	23	0.1115	-2.91E-5
20	0.1104(13)	-0.31E-4(33)	26	0.1107	-2.82E-5
21	0.1096(15)	-0.36E-4(34)	26	0.1099	-2.74E-5
22	0.1067(11)	-0.13E-4(29)	17	0.1091	-2.66E-5
23	0.1103(9)	-0.38E-4(20)	20	0.1084	-2.58E-5
24	0.1083(12)	-0.33E-4(24)	22	0.1076	-2.50E-5
25	0.1088(9)	-0.31E-4(20)	16	0.1069	-2.41E-5
26	0.1092(10)	-0.58E-4(21)	22	0.1062	-2.33E-5
27	0.1056(10)	-0.16E-4(19)	24	0.1054	-2.25E-5
28	0.1075(9)	-0.27E-4(15)	20	0.1048	-2.17E-5
29	0.1072(11)	-0.43E-4(18)	13	0.1041	-2.09E-5
30	0.1033(16)	-0.51E-4(28)	23	0.1034	-2.01E-5
31	0.1039(10)	-0.49E-4(24)	15	0.1027	-1.93E-5
32	0.1021(12)	-0.39E-4(23)	18	0.1021	-1.85E-5
33	0.1014(14)	-0.10E-4(29)	19	0.1014	-1.77E-5
34	0.1019(14)	-0.53E-4(27)	24	0.1008	-1.69E-5
35	0.1002(8)	-0.20E-4(19)	15	0.1002	-1.61E-5
36	0.0987(9)	-0.26E-4(18)	26	0.0996	-1.53E-5
37	0.1001(15)	-0.80E-4(50)	22	0.0990	-1.44E-5
38	0.1000(10)	-0.43E-4(16)	19	0.0984	-1.36E-5
39	0.0999(11)	-0.65E-4(27)	19	0.0979	-1.28E-5
40	0.1000(11)	-0.33E-4(20)	19	0.0973	-1.20E-5
41	0.0973(16)	-0.81E-4(68)	17	0.0967	-1.12E-5
42	0.0952(9)	-0.30E-4(19)	18	0.0962	-1.04E-5
43	0.0963(10)	-0.85E-4(22)	27	0.0957	-9.60E-6
44	0.0942(25)	-0.18E-4(43)	20	0.0952	-8.79E-6
45	0.0945(12)	-0.20E-4(34)	22	0.0947	-8.61E-6

46	0.0970(17)	-0.59E-4(31)	22	0.0942	-8.51E-6
47	0.0970(17)	-0.64E-4(36)	15	0.0937	-8.37E-6
48	0.0935(12)	-0.90E-4(32)	14	0.0933	-7.56E-6
49	0.0939(12)	-0.31E-4(21)	10	0.0928	-7.40E-6
50	0.0915(26)	-0.62E-4(74)	17	0.0924	-7.21E-6
51	0.0919(17)	-0.16E-4(32)	9	0.0919	-7.14E-6
52	0.0925(39)		13	0.0915	-7.03E-6
53	0.0933(38)		13	0.0911	-7.01E-6
54	0.0911(57)		14	0.0907	-6.90E-6
55	0.0889(82)		8	0.0903	-6.88E-6
56	0.0852(65)		9	0.0900	-6.87E-6
57	0.0873(78)		8	0.0896	-6.87E-6
58	0.0901(36)		5	0.0893	-6.86E-6
59	0.0879(41)		4	0.0889	-6.82E-6
60	0.0879(53)		5	0.0886	-6.80E-6
61				0.0883	-6.79E-6
62				0.0880	-6.75E-6
63				0.0877	-6.74E-6
64				0.0874	-6.72E-6
65				0.0872	-6.71E-6
66				0.0869	-6.70E-6
67				0.0867	-6.69E-6
68				0.0865	-6.37E-6
69				0.0862	-6.00E-6
70				0.0860	-5.65E-6
71				0.0858	-5.54E-6
72				0.0857	-5.08E-6
73				0.0855	-4.94E-6
74				0.0853	-4.65E-6
75				0.0852	-4.31E-6
76				0.0851	-4.27E-6
77				0.0849	-3.81E-6
78				0.0848	-3.07E-6
79				0.0847	-2.58E-6
80				0.0846	-2.00E-6